Peculiarities of the photoluminescence of metastable Ga(N,As,P)/GaP quantum well structures

C. Karcher,[*] K. Jandieri, B. Kunert, R. Fritz, M. Zimprich, K. Volz, W. Stolz, F. Gebhard,
S. D. Baranovskii, and W. Heimbrodt

Department of Physics and Material Sciences Center, Philipps University Marburg, D-35032 Marburg, Germany
(Received 8 October 2010; published 8 December 2010)

The metastable quaternary Ga(N,As,P) has been studied experimentally as well as theoretically as promising material for integration of optoelectronics with Si-based microelectronics. The optical studies reveal unusual peculiarities in the photoluminescence response and its temperature dependence. The disorder-induced features have been analyzed by means of Monte Carlo simulations. A two-energy-scale approach is necessary to achieve a satisfactory agreement between experiment and simulation.

I. INTRODUCTION

In recent years much attention has been paid to the study of dilute nitride III-V alloys, both because of their potential for application in optoelectronic devices and their unique physical properties. Band-gap engineering is achieved in these alloys by incorporating a small amount of nitrogen. Nitrogen is an isovalent impurity which differs considerably in size and electronegativity from the substituted anion. If the nitrogen impurity states lie resonantly in the conduction band a strong redshift of the fundamental band gap occurs. For example, by introducing only 2% N in GaAs, a reduction in the band-gap energy of about 250 meV can be achieved.[1,2] The anticrossing interaction between localized nitrogen states and the extended states of the semiconductor matrix splits the conduction band into two subbands: E_+ and E_-.[3,4] The lower E_- subband determines the fundamental band gap.

Basically, the anticrossing behavior opens a wide possibility for the fabrication of long wavelength lasers and light-emitting diodes in the $1.3-1.55$ μm range using, e.g., (Ga,In)(N,As) on GaAs substrate.[5] A set of discrete band gaps has been found in (Ga,In)(N,As) with about 40 meV energy separation due to the different nearest-neighbor environments of nitrogen.[6] Another challenging task is the integration of dilute nitride III-V compounds in monolithic optoelectronic integrated circuits on Si substrates. But the situation is more complicated in case of providing an efficient direct laser material. Silicon itself is not a good candidate because of its indirect band gap. The fabrication of GaAs or (Ga,In)(N,As) lasers on silicon substrate is rather difficult due to the large lattice mismatch of these materials. The indirect semiconductor GaP, however, has a lattice constant almost equal to that of Si. That is why ternary Ga(N,P) can be grown perfectly lattice matched on Si using 2% nitrogen. Moreover, it was claimed in an early paper that already a small amount of nitrogen ($\sim$0.5%) changes the nature of the fundamental band gap of GaP from an indirect to a direct one.[7] Unfortunately, the situation is different as nitrogen forms an in-gap state in GaP. As we could show recently various N-cluster states occur in dependence on the N content which exhibit a rather wide energy distribution and the anticrossing interaction leads to a blueshift of the GaP conduction-band minimum.[8] A much more appropriate material is the quaternary Ga(N,As,P). The GaAs-based alloy is a

direct semiconductor and the lattice parameter can be adjusted to fit the GaP or Si lattice parameter by variation in the N and P content.[9–12]

The application of quantum well (QW) structures in optoelectronic devices requires detailed knowledge of their optical properties and crystallographic quality. The Ga(N,As,P) material system like the other mixed III-(N,V) material systems is metastable due to the large difference in the covalent radius between the Nitrogen and the group V elements (As,P), which are replaced by the N. This metastability can lead to phase separation or other structure formation processes, if growth conditions are not optimized specifically. Even in case of a random distribution of the N ions strong potential fluctuations are anticipated due to the strong differences in size and electronegativity. Disorder and potential fluctuations gives rise, however, to carrier localization that dramatically affects the optical properties.

Photoluminescence (PL) response and absorption measurements are standard tools for characterizing the quality of the sample. In case of disorder-induced potential fluctuations carrier localization takes place and the PL peak energy and the PL linewidth demonstrate typically nonmonotonous temperature dependencies depicted schematically in Fig. 1. The main experimentally observed trends of temperature-dependent PL spectra are (i) a blueshift of the PL peak energy in the range of intermediate temperatures, the so-called S-shape behavior; (ii) a maximum of the PL linewidth within a rather narrow temperature range. Monte Carlo simulations of such experimental findings provide valuable information about the energy scale of the disorder, the electronic properties and hence about the quality of QW structures.

The experimentally observed effects of disorder on the dynamics of the carriers can be reproduced within a model where spatially localized excitons hop between localized states which are distributed randomly in space and energy. Such model has been developed by Baranovskii and Eichmann (BE model in the following).[13] The BE model was successfully applied to various QW systems: (Zn,Cd)Se/ZnSe,[13] (Ga,In)(N,As)/GaAs,[14,15] (Ga,In)(N,As)/Ga(N,As),[16] Ga(N,As)/GaAs,[17] as well as used for quantum dots: (Zn,Cd)Se.[18] The simulations well describe the exponential band tail and reveal the interrelations between the scale of the energy distribution of the localized states and particular features of the PL.

We will show in this paper that quaternary Ga(N,As,P)/GaP QW exhibit some peculiarities in the PL spectra which
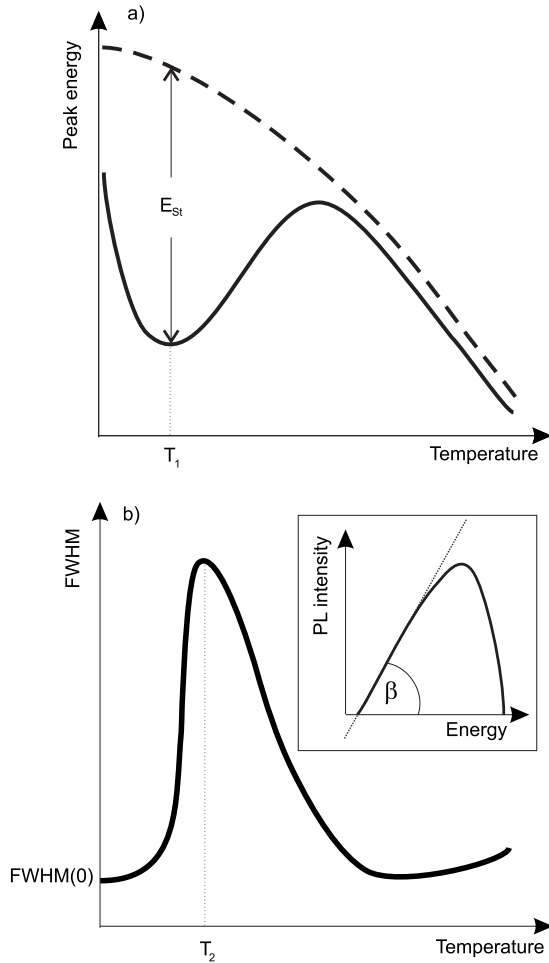
FIG. 1. (a) Schematic representation of the temperature-dependent PL peak position (full line) and the band-gap energy as a function of temperature (dashed line). The deviation between the PL peak energy and the band gap determines the Stokes shift which is caused by the emission from localized excitonic states. T_1 gives the temperature of the maximal Stokes shift. (b) Schematic behavior of the PL linewidth with temperature. T_2 gives the temperature of the maximal PL linewidth. The inset depicts the low-temperature PL spectra with the logarithmic slope β shown by a dotted line.

cannot be explained within a standard BE model. By introducing some modifications we are able to obtain satisfactory agreement between the experimental results and the Monte Carlo simulations.

In Sec. II we present the experimental results. A detailed explanation of the theoretical model and the results of corresponding Monte Carlo simulation are given in Sec. III. We explain in this section step by step the necessary modifications of the BE model to achieve excellent agreement between the experimental results and the model calculations.

II. EXPERIMENT

In order to get insight into the energetic states and respective distribution within the metastable material, we used a combination of photoluminescence and absorption experiments. As for the emissive part, we performed both PL and
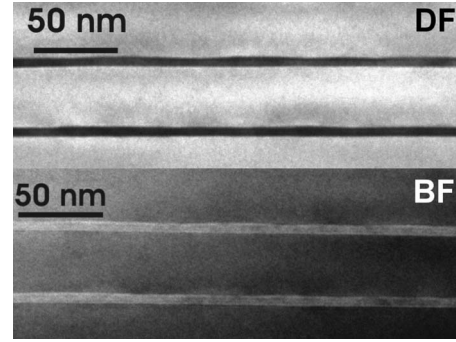

FIG. 2. Dark field (top) and bright field (bottom) TEM image $[g = (002)]$ of a cross section through the Ga(N,As,P) MQW structure. Within the primary quantum well layers a height variation in the quantum well thickness of about 1 nm at a lateral scale of about 100–200 nm can be identified.

PL excitation (PLE) spectroscopy. Since features in linear absorption tend to be rather broad, we used contactless electromodulated reflectance (CER) for the absorptive part of our study. This technique yields well resolved features at critical points in the combined density of states (DOS). With this information we are able to sketch a complete energetic picture, revealing the complex interplay between absorption edge and emission within the quaternary QW system. These investigations will provide the basis for the precise theoretical description in Sec. III.

A. Structural and experimental details

The $Ga(N_{0.04}As_{0.91}P_{0.05})/GaP$ structure used for this study is a typical specimen for a series of Ga(N,As,P)/GaP QWs which have been grown on (001)-oriented GaP substrate by metal-organic vapor-phase epitaxy (MOVPE). Details of the MOVPE growth conditions have been given earlier.[19] The sample has been grown pseudomorphically strained with respect to the substrate, consisting of three quantum wells with a width of 6.7 nm each within 100 nm GaP barriers. The N concentration is 4% and the P content is 5%. Although the incorporation of both phosphorus and nitrogen decreases the lattice mismatch between GaP and the GaAs-based quaternary alloy, there is still a mismatch of about 2.5%. Hence the quantum wells are compressively strained between the GaP barriers which has to be taken into account when interpreting the internal transitions within the quantum well.

Figure 2 shows a cross-sectional dark field and a bright field transmission electron microscopy (TEM) micrograph of the quantum well structure under investigation here. It can be seen that although the Ga(N,As,P) quantum well is coherently strained, there is no sign of relaxation or extended defect formation. Detailed investigations of several images allow the conclusion that the upper quantum well interface with the GaP barrier has a height variation of about 1 nm. The lateral length scale of this well width fluctuation is in the range of 100–200 nm. As has been shown earlier deviations from a random N distribution cause microscopic strain fields, which originate from a chainlike N ordering and result in thickness fluctuations of the QWs.[20] Figure 2 clearly illus-
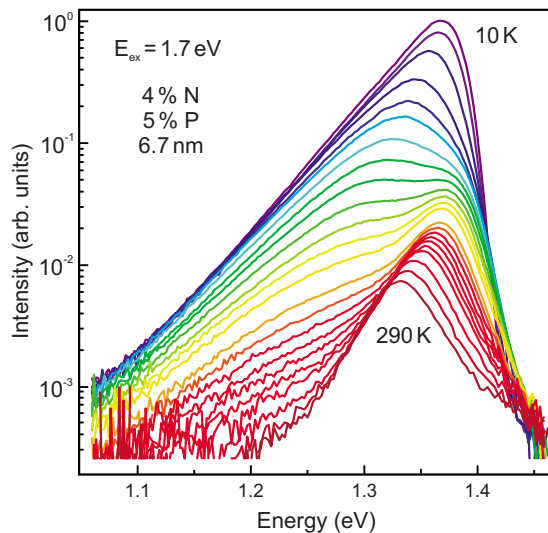
FIG. 3. (Color online) Temperature-dependent photoluminescence of the Ga(N$_{0.04}$As$_{0.91}$P$_{0.05}$)/GaP MQW structure, varying from 10 K (top) to 290 K (bottom).
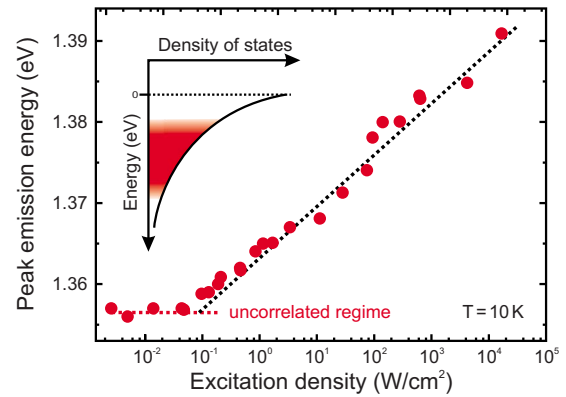

FIG. 4. (Color online) Excitation density dependence of the peak emission energy. Upon reaching a critical excitation density, the excitonic emission starts to show saturation behavior, pushing the emission energy higher with increasing excitation density.

trates that this fluctuation in height even increases when growing multiquantum wells. The modulation is more pronounced in the upper well.

Both PL and PLE measurements were performed using a Spectra-Physics Model 3900S CW Ti:sapphire laser which is able to emit light with a photon energy varying from 1.1 to 1.7 eV. The PL of the sample was measured by means of a standard setup consisting of a 1.25 m grating spectrometer and a liquid-nitrogen cooled germanium detector. The exciting laser is guided through a mechanical chopper in order to amplify the photoluminescence by the standard lock-in technique. The sample was placed in a microcryostat in which temperatures from 10 K up to room temperature can be applied. The electromodulated reflectance was carried out using a cryostat with a sample holder which keeps the sample between a copper block and an indium tin oxide coated glass disk so that external electric fields of up to 50 kV/cm can be applied contactlessly. The reflected light was detected by a Si diode and the modulated reflectance was measured again by lock-in technique.

B. Experimental results

The PL spectra measured at various temperatures in a range from 10 K up to room temperature are shown in Fig. 3. The PL, originating from electron-hole recombination within the Ga(N,As,P) quantum wells, exhibits a maximum around 1.368 eV at room temperature. As predicted by the band anticrossing model, the interaction between localized N states and the conduction band of the Ga(As,P) host results in an energy decrease in the newly formed E_- band.[9] Apart from that overall energetic shift, the photoluminescence shows a complex temperature dependence. Although the band-gap energy of semiconductors usually tend to decrease with increasing temperature due to a larger interatomic spacing and enhanced electron-phonon interaction, the observed emission does not behave accordingly (see Fig. 3). Instead of

a monotonic redshift of the PL position with increasing temperature, an initial blueshift can be observed followed by a mixture of redshift and blueshift at higher temperatures. This is the typical S-shape behavior aforementioned which has been reported for a variety of semiconductor solid solutions. The S-shape behavior could be successfully explained and simulated by thermal activated hopping processes assuming an exponentially density of localized states originating from the disorder caused by the statistically distribution of cations and anions. These states are energetically below the mobility edge which separates the extended states from the localized states.

A strong indication of the exponential character of this localized density of states was experimentally found as can be seen in the slope of the peak emission energy in Fig. 4. The excitation density within the sample was varied by increasing the laser intensity, i.e., both increasing the power and reducing the spot size down to 1 μm. Thus, we were able to induce saturation effects within the localized DOS, tuning the emission energy at low temperatures from 1.355 up to 1.39 eV at a rate of about 6 meV per power decade (see Fig. 4). Upon reaching a peak emission energy of 1.355 eV at a comparably low excitation density of about 0.1 W/cm^2, the power dependence of the emission energy vanishes. Further reduction in the excitation density has no impact on the emission spectrum anymore, leading to the plateaulike behavior which can be observed for very low excitation densities in Fig. 4. This behavior can be understood regarding the finite lifetime of the excitation. At these low excitation densities the exciton can hop freely downward between the localized states and is not affected by the presence of other excitons anymore. Two dominating processes which block its way downward in energy are to either get trapped in a localized state where it does not find a neighboring state to hop to or decay radiatively during the hopping process. Both possibilities form the energetically lowest spectrum we observe for low excitation densities. Hence, we call it the uncorrelated regime. When investigating the full temperature dependence of the emission up to room temperature (see Fig. 5), one can follow the filling of the former S shape with increasing excitation density up to a complete vanishing of the non-
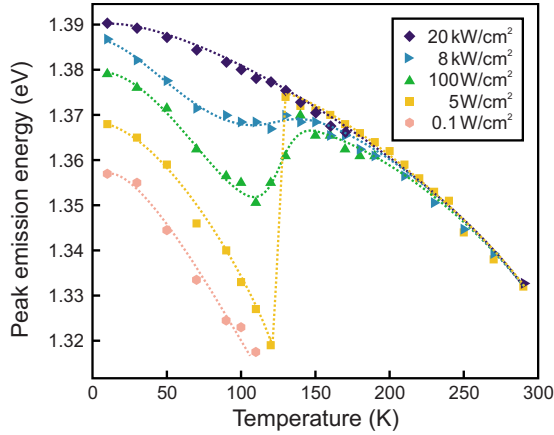
FIG. 5. (Color online) Temperature dependence of the peak emission with varying excitation densities. As the carrier concentration increases, the observed S shape of the luminescence more and more smudges until it completely disappears.

monotonic behavior. For the further studies, we used a low excitation density at about 5 W/cm² where a complete temperature dependence is still detectable.

At first glance, everything seems to follow the expected trend as observed in other highly disordered alloys. There is, however, a remarkable difference between earlier reports and the results reported here. As can be seen in Fig. 3, there is an intermediate temperature range where the PL spectra exhibit two local maxima in parallel. We will come back to this point later.

An important parameter for the theoretical description of the disorder-induced S-shape behavior is the temperature dependence of the mobility edge, which has not been observed in earlier reports. We were able to identify the mobility edge of the system by both temperature-dependent PLE and CER. Since both experiments yield actually identical information, we present here only the temperature dependent CER (see Fig. 6). The CER signal illustrates the energetic position of the first three electronic transitions within the QW. Discrete levels of energy for both confined electrons and holes are
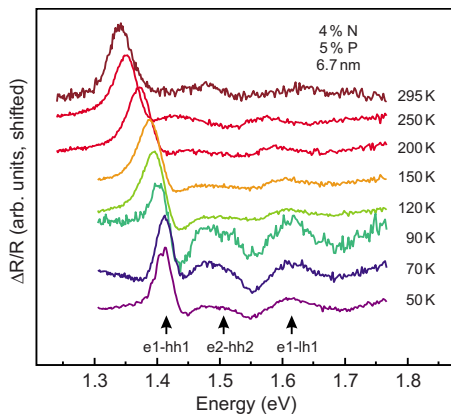

FIG. 6. (Color online) Temperature-dependent electromodulated reflectance of the Ga(N$_{0.04}$As$_{0.91}$P$_{0.05}$)/GaP MQW structure. Apart from the energetically lowest first electron-hole transition within the quantum well, further transitions of higher order can be identified.
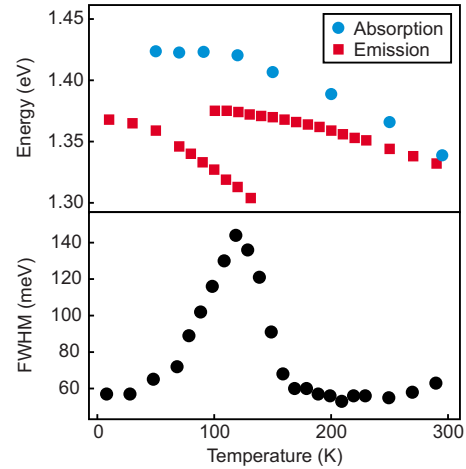

FIG. 7. (Color online) Upper part: temperature dependence of peak emission (see Fig. 3) and absorption (by fitting the first transition obtained from the CER measurements to the standard lineshape model, see Fig. 6). Lower part: temperature dependence of the linewidth of the emission.

formed according to the well width of the Ga(N,As,P) layer of 6.7 nm. Transitions between these states can be observed in the CER spectrum as derivativelike features. As aforementioned, the Ga(N,As,P) layer is biaxially compressively strained, leading to a splitting of the formerly degenerate light- and heavy-hole subbands by about 200 meV. Hence, the first observed transition within the QW originates from a transition between the energetically lowest electron and the heavy-hole subbands. By fitting the signals to a first derivative line-shape model,[21] we are able to estimate the energetic positions of the transitions. In the framework of a straightforward QW calculation including Coulomb interaction we were able to reveal the transitions as e1-hh1, e2-hh2, and e1-lh1, as depicted in Fig. 6.

For the following study, we limit our observation onto the energetically lowest lying transition between the first electronic and the first heavy-hole subband (e1-hh1). Actually, this is the mobility edge for the QW excitons. The temperature-dependent measurements enable a direct observation of the variation in the mobility edge with increasing thermal energy of the lattice. The results are depicted in the upper part of Fig. 7. The energetic positions of the PL maxima are given by full squares as function of temperature and the lowest absorption transition is depicted vs temperature as full circles. While the energy of the mobility edge of the system decreases monotonously by rising the temperature, the PL maximum rather resembles the typical S shape. In the lower part of Fig. 7, the total linewidth of the PL is given, neglecting the two local maxima in the intermediate temperature range. It is noteworthy that the linewidth of the emission more than doubles up to a value of 144 meV and then decreases back to its original width around 55 meV from where it slightly increases to about 63 meV at room temperature.

As the following theoretical part will demonstrate, these experimental results cannot fully be simulated by simply applying the previously introduced BE model. One possible reason for that can be identified when looking at the cross-

sectional TEM images of Ga(N,As,P) QWs (see Fig. 2). Apart from a concentration fluctuation on the atomic scale, a thickness fluctuation of about 1 nm along the QW can be identified. This fluctuation has a lateral extension of about 100–200 nm, forming a second source of disorder within the quaternary multiquantum well (MQW) structure. This second scale has to be taken into account when modeling the system theoretically in Sec. III.

III. THEORETICAL MODELS AND SIMULATION RESULTS

As afore mentioned the theoretical model suggested in Ref. 13 was successfully applied to many QW systems. The model assumes that the disorder can be characterized by a single spatial scale of disorder and a respective energy distribution of the localized states. In Sec. III A we start our investigation by applying the BE model. We will discuss some possible modifications of the standard model and will show that still discrepancies remain between experiment and simulation. In Sec. III B we introduce a second disorder scale by dividing the QW into cells. We found that even this is not sufficient if we restrict the excitonic mobility to the respective cells. In Sec. III C we discuss the parameters of the transition probability between the cells to achieve a satisfactory agreement between the experimental data and the Monte Carlo simulations.

A. Theoretical description with one scale of disorder

1. Baranovskii-Eichmann model

The main features of the BE model[13] are the following. The alloy composition and imperfect interfaces between the quantum well and surrounding barriers create disorder. Excitons generated by optical excitation are captured into the respective randomly distributed localized states, which may act as radiative recombination centers. The total PL is conditioned by the recombination and hopping kinetics of the captured excitons.[22] Excitons have some typical lifetime τ_0 with respect to radiative recombination. During its lifetime the excitons can perform phonon-assisted transitions which are described by the Miller-Abrahams tunneling rates.[23] The hopping transition rate from an occupied site i to an empty site j over a distance R_{ij} is given by

$$\nu_{ij} = \nu_0 \exp\left(-\frac{2R_{ij}}{\alpha} - \frac{E_j - E_i + |E_j - E_i|}{2k_B T}\right), \quad (1)$$

where E_i and E_j are the energies of sites i and j, respectively, T is the lattice temperature, k_B is the Boltzmann constant, α is the localization length, that is the decay length of the localized exciton center-of-mass wave function, and ν_0 is the attempt-to-escape frequency.

In a quasi-two-dimensional (2D) QW the problem reduces considerably. If one considers a 2D rectangle of the linear size $L = N_0^{-1/2}$ containing N_0 trapping sites and employ the periodic boundary conditions, the first term in the exponent of Eq. (1) can be written as $\exp(-2r_{ij}/\sqrt{N_0 \alpha^2})$, where $r_{ij} = R_{ij}/L$ is the distance between the sites i and j measured in

TABLE I. E_0 characteristic energies (third column) extracted from the experimentally observed (second column) PL features using the corresponding universal relations (first column) of the theoretical model with one-scale exponential DOS.

Relation between E_0 and PL features	PL feature (meV)	E_0 (meV)
$k_B T_1 = (0.75 - 0.80)E_0$	10.4	13
$k_B T_2 = (1.10 - 1.15)E_0$	10.4	9
$\text{FWHM}(0) = (2.5 - 2.7)E_0$	57	22
$\beta = E_0^{-1}$	0.025[a]	40

[a]The value of β is given in (meV)$^{-1}$.

the units of L. $N_0 \alpha^2$ and $\nu_0 \tau_0$ are the important parameters of the model.

Beside the hopping, the possibility of thermal activation into extended states above the mobility edge is also taken into account.[14] The probability of such transitions is given by

$$\nu_a = \nu_0 \exp\left(\frac{E}{k_B T}\right). \quad (2)$$

The energy E is taken positive for extended states and negative for the localized ones. The model furthermore involves the concentration ratio of nonradiative and radiative recombination centers N_{nr}/N_0 as another important simulation parameter. This opens the possibility to simulate the temperature dependence of the integrated PL intensity.[14]

The essential feature of the model is the energy distribution of the localized states. It is assumed that this distribution can be described by some $f(E/E_0)$ function that represents the shape of the band tail and involves a single E_0 characteristic energy scale,

$$g(E) = A f\left(\frac{E}{E_0}\right), \quad (3)$$

where A is the normalization parameter.

The application of this model to various QW systems,[13–17] as well as for quantum dots[18] reveal the exponential shape of the DOS

$$g(E) = \frac{N_0}{E_0} \exp\left(\frac{E}{E_0}\right), \quad (4)$$

as well as some general relations between the E_0 energy scale and the distinct features in the temperature-dependent PL behavior, given in the first column of Table I. Here FWHM(0) is the full width at half maximum of low-temperature PL spectra and T_1 and T_2 are the temperatures corresponding to the maximum of the Stokes shift and FWHM, respectively (see Fig. 1). E_0^{-1} equals the logarithmic slope β of low-temperature PL spectra in its low-energy part (see inset of Fig. 1). This relation can be justified by simple physical considerations. Indeed, at low temperatures the photoluminescence intensity from sufficiently deep trapping sites follows the shape of the DOS.

If the values E_0 determined by means of the different universal relations given in Table I are in reasonable agreement with each other, one can conclude that the BE model describes the PL of a given system adequately. This was the case for the earlier investigated QW structures[13–17] (for example, the values of E_0 extracted from various PL features of (Ga,In)(N,As) QW structures[16] were 9 meV, 7 meV, 6 meV, and 8 meV, respectively), however, here we do observe significant deviations in the determined values of E_0.

2. Simulation with an exponential DOS

We start our test by applying the universal relations given in the first column of Table I on the experimental data of our Ga(N,As,P)/GaP QWs (see Fig. 7). In the second column the experimental data are given, whereas in the third column the resulting E_0 values are given. It is obvious that the values determined from T_1 and T_2, corresponding to the Stokes shift and the PL linewidth, respectively, are in good agreement. They deviate considerably, however, from the E_0 values determined from the low-temperature PL features FWHM(0) and β. On the basis of this rather serious discrepancy we have to conclude already that our experimental results cannot be modeled by the standard BE model. Nevertheless we performed Monte Carlo simulation, which confirm this conclusion. The simulation results (open circles) are compared to the experimental values (full circles) in Figs. 8(a) and 8(b). The values used in the simulation are $E_0 = 10$ meV and $N_0\alpha^2 = 0.5$ and $\nu\tau_0 = 5 \times 10^3$. It is obvious that the characteristic features corresponding to T_1 and T_2 are well represented by $E_0 = 10$ meV as expected. The absolute value of the FWHM(0) is, however, much too small. This is confirmed by comparing the calculated PL (dashed line) with the experimental PL (full line) in Fig. 8(c). The logarithmic slopes differ significantly. It should be mentioned that the variation in $N_0\alpha^2$ and $\nu_0\tau_0$ parameters does not improve the fitting.

We have to conclude that the standard BE model with just a single exponential DOS is not applicable. It might be possible, however, that the assumption of a pure exponential DOS is oversimplified. In order to check this, we performed Monte Carlo simulations using reasonable modifications. The results are given in what follows.

3. Simulation using a modified exponential DOS function

As aforementioned, the experimentally observed PL exhibits an exponential slope at the low-energy side at low temperatures [see solid line in Fig. 8(c)]. As discussed in Sec. III A 1, the PL intensity from the sufficiently deep trapping sites follows the shape of the DOS. This excludes the Gaussian density of states as a possible candidate to fit our experimental data. Therefore, we at first tried a modified exponential function given by

$$g(E) = A \exp\left[-\left|\frac{E}{E_0}\right|^\gamma\right]. \quad (5)$$

Here A is a normalization factor and γ is a fitting parameter. In Fig. 9 the resulting slopes of $g(E)$ are depicted for $E_0 = 10$ meV and various γ values in comparison with the pure exponential function with $E_0 = 40$ meV. It is obvious
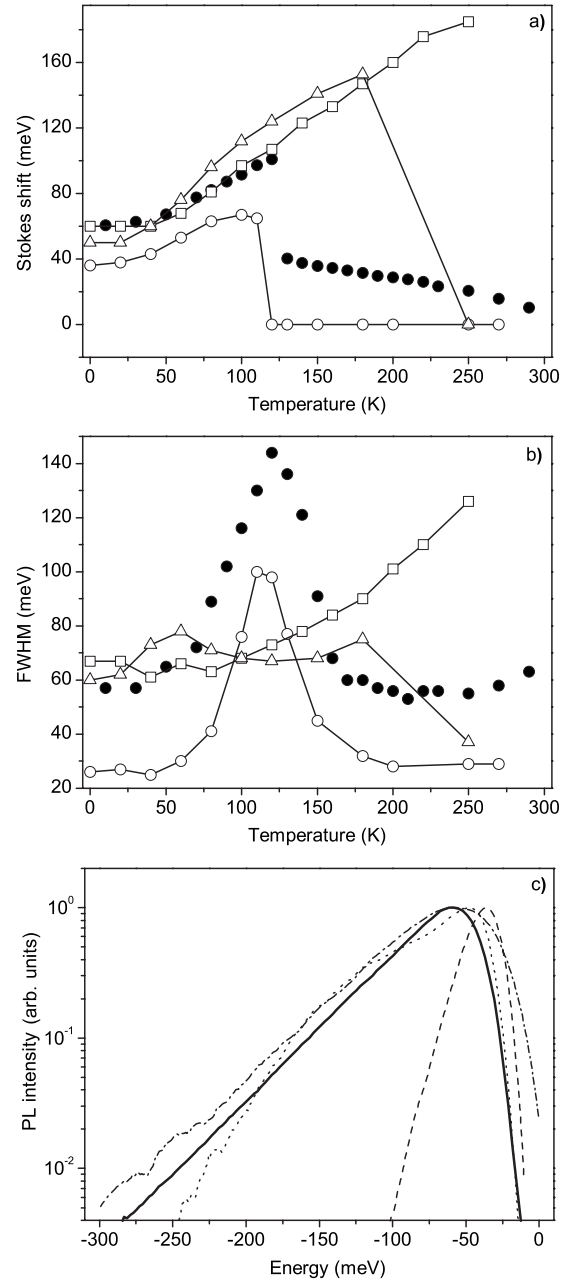

FIG. 8. Temperature dependencies of (a) the Stokes shift and (b) FWHM of Ga(N,As,P)/GaP QWs. (●) Experimental points taken from Fig. 7. (○) Theoretical simulation using Eq. (4). (□) Simulation using Eq. (5) with $\gamma = 2/3$. (△) Simulation using Eq. (6). (c) PL spectra at low temperatures. (Full line) Experimental curve taken from Fig. 3; (dashed line) simulation with Eq. (4); (dashed-dotted line) simulation Eq. (5) with $\gamma = 2/3$; and (dotted line) simulation with Eq. (6). See text for details.

that the slope coincides at best for $g(E) = A \exp[(E/E_0)^{2/3}]$. The resulting low-temperature PL obtained by Monte Carlo simulation is shown in Fig. 8(c) as dashed-dotted line. As anticipated, a nice agreement can be achieved with the experimental PL. In Figs. 8(a) and 8(b) the obtained Stokes shift and the PL linewidth are depicted as open squares. As can be seen neither the Stokes shift nor the PL linewidth can be fitted well.
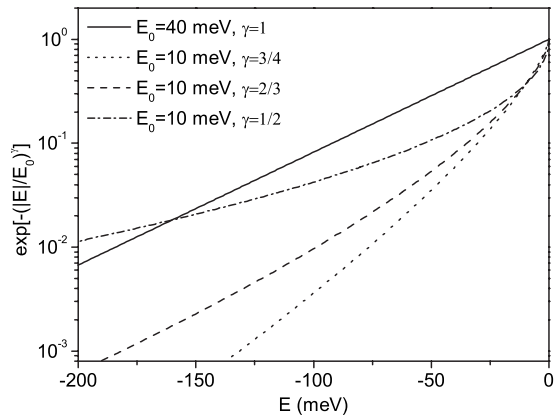
FIG. 9. The function $\exp[(E/E_0)^\gamma]$ for various values of E_0 and γ. See text for details.

As an alternative modification we therefore tried a combined density of states consisting of an exponential distribution with the energy scale E_0 and a Gaussian distribution with the mean value E_m and the standard deviation σ. The general form of such energy distribution is given by

$$g(E) = A \left\{ \exp\left(\frac{E}{E_0}\right) + B \exp\left[\frac{(E - E_m)^2}{2\sigma^2}\right] \right\}, \quad (6)$$

where A is again a normalization parameter and B determines the ratio between the exponential distribution of the localized states and those distributed according to a Gaussian shape. The main idea of this approach is to unify the temperature dependencies of the Stokes shift on the one hand and the PL linewidth on the other hand.

We performed Monte Carlo simulation using Eq. (6) with various sets of fitting parameters E_m, σ, and B. A typical result is depicted in Figs. 8(a) and 8(b) as open triangles for the Stokes shift and of the PL linewidth simulated with $N_0\alpha^2 = 1.0$, $\nu_0\tau_0 = 10^4$, $E_0 = 10$ meV, $E_m = 0$, $\sigma = 70$ meV, and $B = 0.028$. The corresponding low-temperature PL spectra are given in Fig. 8(c) as dotted line. Again, the low-temperature PL can be fitted well while the disagreement in Figs. 8(a) and 8(b) is striking. We can conclude that even for sensible modifications of the DOS the BE model[13] cannot be directly applied for the theoretical explanation of the PL behavior of Ga(N,As,P) compounds.

B. Theoretical model with two different scales of disorder (extended Baranovskii-Eichmann model)

In this section we will show that the extension of the one-scale picture by introducing a second energy scale is the necessary improvement to enable the satisfactory simulation of all important PL features of Ga(N,As,P)/GaP QW structures.

So far our theoretical approach based on the BE model assumed that each exciton has an identical energy distribution of the localized states within reach regardless of its spatial position. In this case a single spatial disorder scale and a respective single energy scale is appropriate.

The source of that single energy scale is assumed to be the random distribution of the N atoms on anion site. We have

seen in Fig. 2 that we are faced with a second disorder scale given by the thickness fluctuations of the QW. These thickness fluctuations act as localization sites for the excitons with a rather large lateral localization length. This motivates the introduction of a second scale of energy distribution.

Such an approach was used earlier in Refs. 24–26 to explain an unusual large linewidth of the low-temperature PL spectra in AlInGaN quaternary bulk material and InGaN multiple quantum wells. In these papers Gaussian distribution of the localized states in both length scales have been used. Recently, a two length scale has been used to account for clustering effects in Ga(As,Bi).[27] In this paper an exponential distribution has been combined with a Gaussian distribution. In the following we use the two-scale model but with two exponential instead of Gaussian distribution since we have to account for the well-pronounced exponential shape of the low-temperature PL.

1. General description of the model

We assume that the long-range disorder potential exhibits a spatial scale which is comparable or larger than the area that an exciton can explore during its lifetime. This long-range potential is schematically shown in Fig. 10(b). We assume furthermore an additional short-range disorder at much smaller spatial scale depicted in the inset of Fig. 10(b). The long-range disorder potential can be represented as a steplike function [thin line in Fig. 10(b)]. As a result, the QW layer can be considered as a sequence of rectangular elements. These cells are depicted schematically in Fig. 10(a). Within each cell the long-range disorder potential is constant defining the effective mobility edge for the localized states conditioned by the short-range disorder. The energy distribution of the long-range disorder potential steps is given by

$$g_1(\varepsilon) = A \exp\left(\frac{\varepsilon}{\varepsilon_0}\right) \quad (7)$$

with A the normalization parameter and ε_0 the characteristic energy scale. The energy is measured from some energy level identified with maximal possible effective mobility edge in the sample. Within each cell the energy distribution of the localized states determined by the short-range disorder potential is given by

$$g_2(E - \varepsilon) = B \exp\left(\frac{E - \varepsilon}{E_0}\right) \quad (8)$$

with the normalization parameter B and the characteristic energy E_0.

The simulation algorithm is similar to that described in Sec. III A 1, except for one essential difference: the energy positions of the localized states are determined not only by the short-range energy distribution given in Eq. (8) but also by the effective mobility edges of the cells distributed according to Eq. (7). Therefore, we need two random numbers to determine the localized state that captures the exciton. One random number describes the particular cell and the other one the localized state within this cell.

Using Eqs. (7) and (8), the total-energy distribution of the localized states in the QW layer can be calculated as
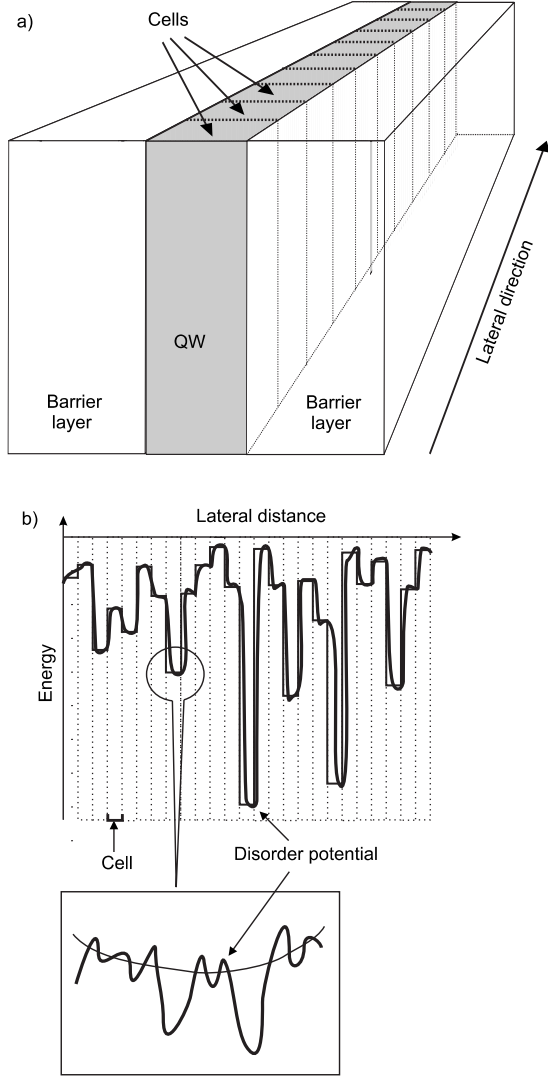
FIG. 10. (a) Schematic representation of the QW layer as a sequence of cells, (b) schematic representation of the long-range disorder potential (solid line) and corresponding steplike function (thin line). Inset: the short-range disorder potential within a single cell.

$$G(E) = C \int_E^0 g_1(\varepsilon) g_2(E - \varepsilon) d\varepsilon, \qquad (9)$$

where the normalization parameter C can be determined from the constant number N_0 of localized states

$$\int_{-\infty}^0 G(E) dE = N_0. \qquad (10)$$

The total DOS of the localized states is then

$$G(E) = \frac{N_0}{\varepsilon_0 - E_0} \left[\exp\left(\frac{E}{\varepsilon_0}\right) - \exp\left(\frac{E}{E_0}\right) \right]. \qquad (11)$$

According to Eq. (11), for sufficiently low values of E the density of states is determined by a single exponent with energy scale E_0 or ε_0, depending which of them has the larger value. In what follows we will show that the DOS

given by Eq. (11) provides the opportunity to meet all the important PL features which have been experimentally observed. It is worth mentioning that using a DOS according to Eq. (11) allows for a unique determination of E_0 and ε_0 using the experimental values of T_1, T_2, and β.

Let us now discuss the resulting Stokes shift. According to Eq. (11), the total-energy distribution of the localized states has a maximum at energy E_c given by

$$E_c = \frac{\varepsilon_0 E_0}{\varepsilon_0 - E_0} \ln\left(\frac{\varepsilon_0}{E_0}\right) \qquad (12)$$

and even without hopping transitions, the low-temperature Stokes shift has a nonzero E_c value. In real situations, the low-temperature Stokes shift is determined of course by both the maximum of the total-energy distribution and the hopping transitions between the localized states within each individual cell. As a result, its value will be equal at least to the sum of $E_{St}(0)$ and E_c, determined by Eq. (12). Therefore, the experimentally determined value of the low-temperature Stokes shift enables the determination of all possible pairs of simulation parameters ($N_0\alpha^2$ and $\nu_0\tau_0$) since the values of E_0 and ε_0 and hence, the value of E_c are fixed by the experimentally observed T_1, T_2, and β. The unique determination of the correct pair of $N_0\alpha^2$ and $\nu_0\tau_0$ is possible using the temperature dependence of the integrated PL intensity. As mentioned in Sec. III A 1, according to Ref. 14, the temperature behavior of integrated PL intensity can be simulated taking into account the thermal activation of localized excitons into the extended states above the mobility edge and their recapture either by radiative or nonradiative recombination centers. This latter process reduces the PL efficiency and hence the integrated PL intensity. The activation probability is an exponential function of the localization energy. Since the hopping and recombination probabilities are sensitive to the pairs of $N_0\alpha^2$ and $\nu_0\tau_0$ even the integrated PL intensity and its temperature behavior will be sensitive to these parameters. Additionally, the simulation of the temperature-dependent integrated intensity opens the possibility to determine another important material parameter, namely, the concentrations ratio of nonradiative and radiative centers N_{nr}/N_0.

Basically, the model with two disorder scales allows for a description of all the important experimental findings. The Monte Carlo simulation based on this model opens the possibility of an unambiguous determination of important material parameters such as: characteristic energy scales of the disorder, exciton lifetimes, the combination of exciton localization length and the concentration of localized states as well as the concentration ratio of nonradiative and radiative centers.

2. Simulation results

Using the model with two scales of disorder we now simulate the PL behavior of the Ga(N,As,P)/GaP QW structure. The experimental values of T_1 and T_2 [see Figs. 8(a) and 8(b)] yield the characteristic energy of the short-range distribution $E_0 = 10$ meV, whereas the logarithmic slope of the low-temperature PL spectra gives the energy scale of the
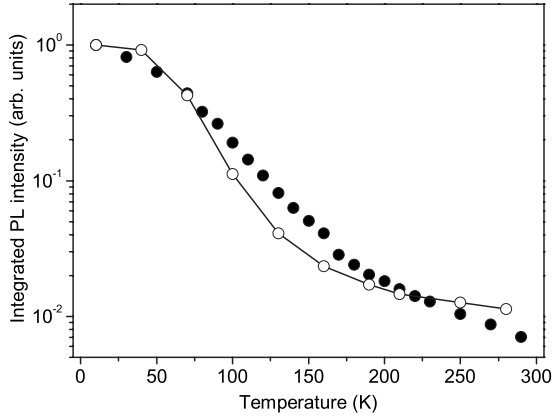
FIG. 11. Integrated PL intensity as function of temperature of a Ga(N,As,P)/GaP QW. (●) Experimental points and (○) simulated results.

long-range disorder $\varepsilon_0 = 40$ meV. The simulation parameters $N_0 \alpha^2$ and $\nu_0 \tau_0$ are determined by the experimentally observed low-temperature Stokes shift and by the temperature dependence of the integrated PL intensity shown in Fig. 11 (●). Best agreement between simulated (open symbols in Fig. 11) and the experimental points was achieved for $N_0 \alpha^2 = 0.5$ and $\nu_0 \tau_0 = 5 \times 10^3$ and for $N_{nr}/N_0 = 0.03$ being the concentrations ratio of nonradiative and radiative centers.

The simulation results are given in Fig. 12. The calculated Stokes shift and the PL linewidth are depicted in Figs. 12(a) and 12(b) by stars. The experimental points are the full circles. It is obvious that the main experimental characteristics are nicely reproduced. The respective PL spectra are depicted in Fig. 12(c) with the expected low-energy slope.

Looking more closely, one can see that despite the satisfactory agreement already achieved the simulated values of the maximal Stokes shift and the maximal PL linewidth are still considerably lower than experimentally observed values. But most importantly, the experimentally observed double structure in the PL did not appear so far.

In the next section we explain the necessary additional modifications of our theoretical model to eliminate even these remaining discrepancies.

C. Two different scales of disorder and finite transitions probability between different cells

In the theoretical model used so far the cells were assumed to be completely separated from each other in the sense that the exciton captured by one cell remains in the cell during its whole lifetime τ_0. No transitions between the cells were allowed. This approximation is justified if the lateral size of the cell is large compared to average the size of the area that can be explored by an exciton during its lifetime. Nevertheless, near the boundaries of the cells there is always some finite transition probability for excitons between the neighboring cells. Basically localized excitons may hop and excitons above the mobility edge may diffuse into the neighboring cell. As the hopping transition is the much slower process we consider only diffusive intercell transfer. We introduce transfer probability $\xi(T, \varepsilon)$ that might be dependent
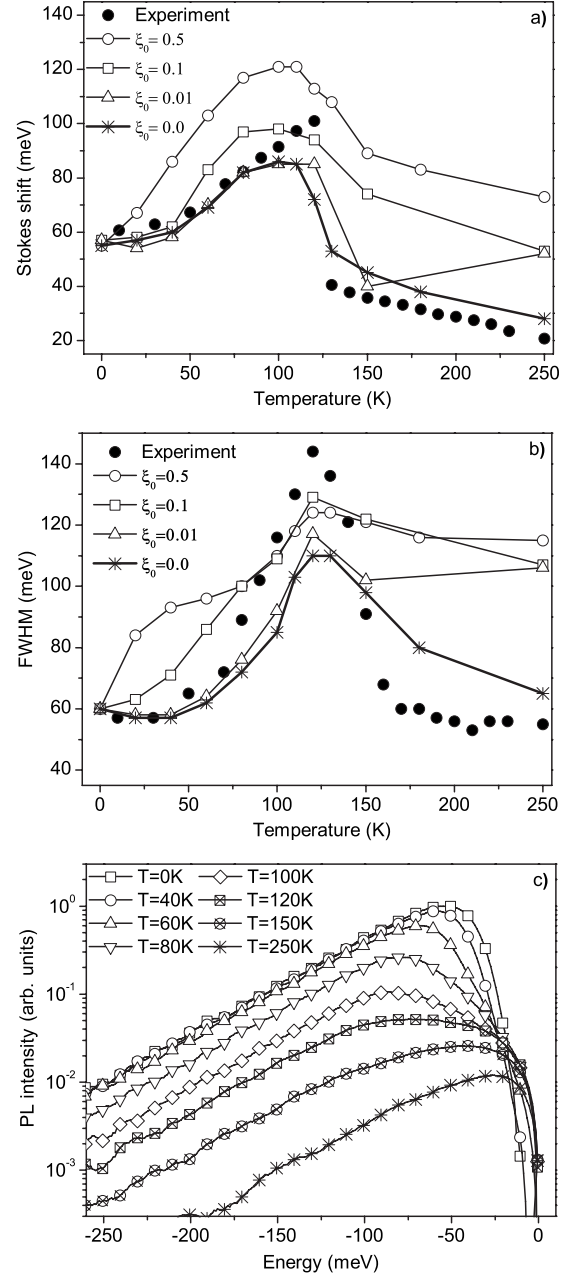

FIG. 12. Temperature dependencies of (a) the Stokes shift and of (b) the FWHM of Ga(N,As,P)/GaP QWs. (●) Experimental points from Fig. 7 and (open symbols) simulation using the model with two scales of disorder and different values of the transition probability ξ_0 between the cells including the case without transitions ($\xi_0 = 0$). The lines are guide for the eyes. (c) PL spectra at various temperatures simulated for $\xi_0 = 0$.

on temperature and also on the effective mobility edge ε of the cell. In the following subsections we discuss in detail which dependencies are needed to reproduce the experimental results in satisfactory manner.

1. Temperature- and energy-independent transitions

We start with the assumption that transitions between the neighboring cells is just a constant $\xi = \xi_0$ without any tem-

perature and energy dependence. Despite of that, some indirect temperature dependence still remains since diffusion transitions become possible only after excitation of localized excitons above the mobility edge. The activation process is an exponential function of the temperature. Furthermore, in case of different effective mobility edges for different cells an upward transition needs some additional activation energy $\Delta\varepsilon = \varepsilon_2 - \varepsilon_1$ and the total probability along with the transition probability ξ will additionally contain the activation multiplier $\exp[-\Delta\varepsilon/k_B T]$. In Figs. 12(a) and 12(b) some curves are depicted for different constant intercell transition probabilities (open symbols). All the other simulation parameters are the same as used before. The simulation results for the maximum of the Stokes shift and of the PL linewidth are higher the larger the intercell transition probability as anticipated. Nevertheless the overall agreement between the experimental results and the simulation becomes poor.

2. Temperature-dependent transitions

Two temperature-dependent factors have essential influence on the intercell transition probability: (i) the exciton thermal velocity and (ii) the exciton scattering at imperfections of the QW-barrier interface. The thermal velocity, being an increasing function with temperature, promotes the transition process. On the contrary, scattering events reduce the intercell transitions by reducing the exciton mobility. Even scattering is higher the higher the temperature. Thus, these two factors work in opposite directions yielding a rather complicated may be even nonmonotonic temperature dependence.

Using this implication and the experimental temperature variations in Stokes shift and linewidth one can construct the temperature dependence of the transition probability shown in the inset of Fig. 13(a), which provides a satisfactorily agreement between the simulated and experimentally observed PL temperature behavior of Ga(N,As,P)/GaP QW [see open circles in Figs. 13(a) and 13(b)]. The corresponding PL spectra are depicted in Fig. 13(c). It is important to notice that even with such a complicated temperature dependence of the intercell transition probability we are not able to reproduce the PL structure with two maxima in the intermediate temperature range.

3. Temperature- and energy-dependent transitions

As a next step we introduce a possible energy dependence. As aforementioned the intercell transition probability can also depend on the relative positions of the various effective mobility edges ε of the cells.

As shown in Fig. 2 we assume that the sequence of the cells is created by the long-range thickness variations in the QW. Thus, the cells can be treated as QWs of different width with effective mobility edge being lower the wider the well. In addition, the interface imperfections cause the scattering centers damping the mobility and consequently the transition of the excited exciton between the neighboring cells. Scattering processes are, however, more pronounced the narrower the QW, as the thickness fluctuations create stronger potential fluctuations. As a result, the excitonic mobility is higher
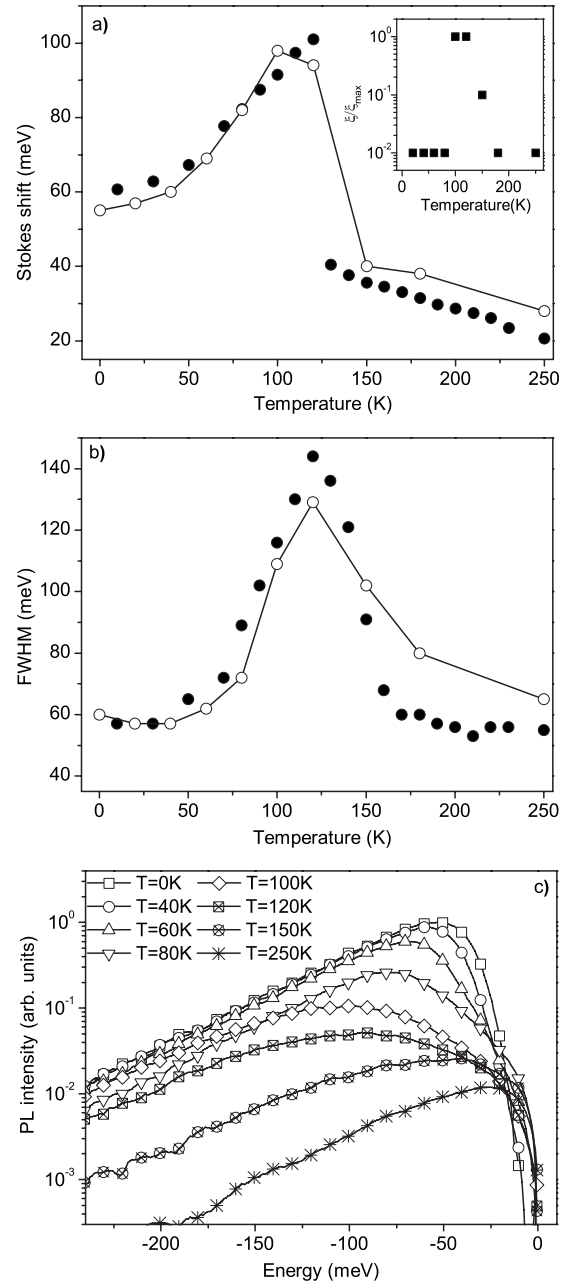

FIG. 13. Temperature dependencies of (a) the Stokes shift and of (b) the FWHM of Ga(N,As,P)/GaP QWs. (●) Experimental points from Fig. 7. (○) Simulation using the theoretical model with two scales of disorder and the temperature-dependent transition probability between the cells shown in the inset of (a). (c) Corresponding PL spectra simulated for various temperatures. All lines are guide for the eye.

in wider QWs and hence the transition probability is an increasing function with the QW width or decreasing function of ε.

We take into account now the temperature and energy dependence of the transition probability in the following manner: each value of the temperature T defines some threshold $\varepsilon_{th}(T)$ value such that for all cells with comparatively wide QW and hence, with comparatively low $\varepsilon < \varepsilon_{th}(T)$ energy, exciton transitions from this cell into the
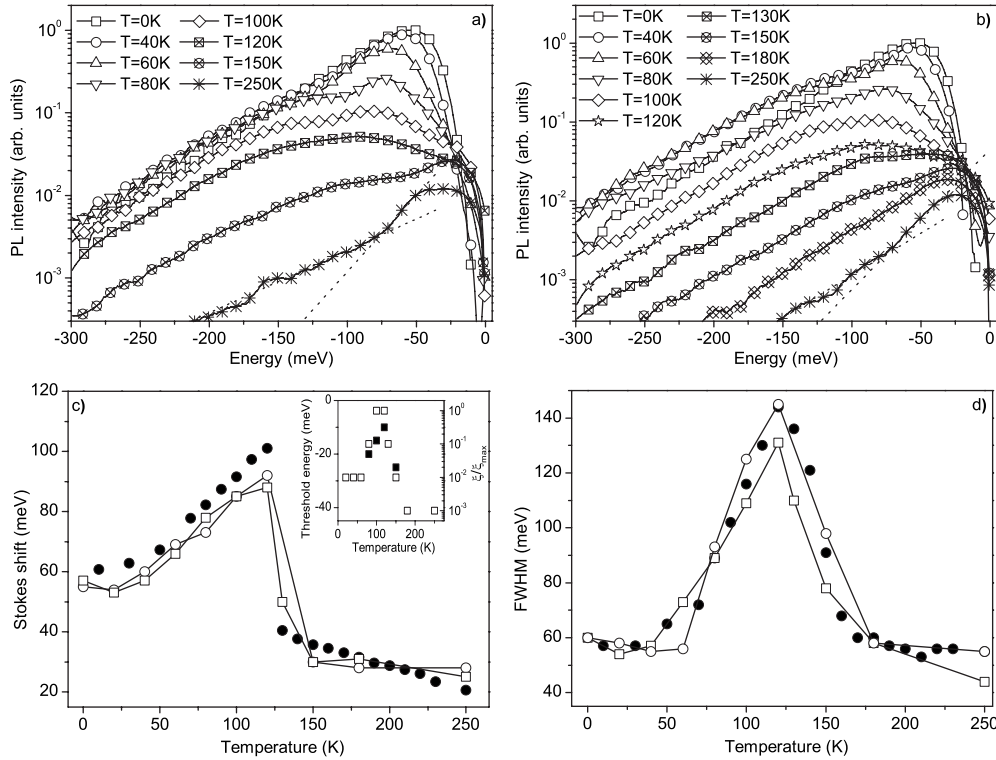
FIG. 14. PL spectra at various temperatures simulated for Ga(N,As,P)/GaP QW simulated by means of the theoretical model with two scales of disorder as well as temperature- and energy-dependent transition probabilities between the cells. (a) Abrupt energy limits for the transition probability with the corresponding $\xi_0(T)$ dependence shown by filled squares in the inset of (c); (b) continuous energy-dependent transition probabilities with the corresponding $\xi_0(T)$ dependence shown by open squares in the inset of (c). (c) Temperature dependencies of the Stokes shift; (d) FWHM; (●) experimental points from Fig. 7. (○) abrupt energy limit for the transition probability; (□) continuous energy-dependent transition probability; lines are just eye guides.

neighboring one are allowed and for all others with comparatively narrow QW transitions are forbidden. As in Sec. III C 1, the $\varepsilon_{th}(T)$ dependence is determined by the thermal velocity of the excitons and by their scattering at the interface imperfections.

The simulation results are depicted in Fig. 14. Again a satisfactory agreement has been achieved with the experimental values for the temperature dependence of the Stokes shift and PL linewidth [open circles in Figs. 14(c) and 14(d)]. The temperature dependence $\varepsilon_{th}(T)$ is depicted in the inset of Fig. 14(a) (solid squares). For very low and very high temperatures the values of E_{th} threshold energy are assumed to be infinitesimally small so that practically no transitions are allowed. The corresponding PL spectra for various temperatures are shown in Fig. 14(a). Obviously we can now simulate at least qualitatively the two PL maxima in the intermediate temperature range as it can be seen by comparison of the PL spectra simulated for $T=80$ and 100 K temperatures [down triangles and diamonds in Fig. 14(c), respectively] with the PL spectra measured at $T=90$ and 100 K (see Fig. 3).

So far we assumed an abrupt energy limit, defined by the threshold energy $\varepsilon_{th(T)}$ for the cells with possible intercell transitions and those where the transitions are completely forbidden. A more realistic consideration would be to assume that the transition probability is a continuous function of ε. According to Ref. 28, in realistic QW samples the interface-

roughness scattering is the dominant mechanism in limiting the diffusivity and the diffusivity increases exponentially with increasing the width of the well, that is, with decreasing the ground energy. Assuming that the interband transition probability is determined by the ratio of diffusive length and the L_0 linear size of the cell, we introduce the following expression:

$$\xi(T,\varepsilon) = A\xi_0(T)\exp\left(\frac{\sqrt{|\varepsilon|}}{\eta}\right), \qquad (13)$$

for the temperature- and energy-dependent probabilities of the exciton transition from a cell with ε energy into the neighboring cell. A is introduced for normalization purpose and η is a scaling parameter. Best agreement is obtained for $\eta=0.5$ assuming $\xi(T)$ dependencies shown by open rectangles in the insets of Fig. 14(c). The corresponding temperature dependencies of the Stokes shift and PL linewidth is shown by open rectangles in Figs. 14(c) and 14(d). The PL spectra for various temperatures are given in Fig. 14(b). It is obvious that for these more realistic conditions we also can simulate the double structure in the experimental PL.

IV. CONCLUSIONS

The photoluminescence behavior of quaternary Ga(N,As,P)/GaP QW structure is studied experimentally and

theoretically. The experimental investigations reveal several peculiarities in PL response and its temperature dependence unusual for other III-V compounds including ternary dilute nitride alloys. Namely, (i) two different energy scales were found when comparing the logarithmic slope of low-temperature PL spectra in its deep energy part and the thermal energy of the respective temperature at which the S shape occurs. (ii) At intermediate temperatures the PL spectra exhibit a complex structure with two maxima. We have shown that the theoretical model suggested in Ref. 13 based on the hopping relaxation of photoexcitations in the band tails of compound semiconductor and assuming the single spatial and energy scales of disorder potential cannot provide the simultaneous explanation of all observed PL peculiarities.

We suggest in this paper a theoretical model with two different spatial and energy scales of disorder potential taking into account the finite lifetime of excitons and their finite lateral velocity being excited from localized into the extended states above the mobility edge. It is assumed that the long-range disorder is conditioned by the long-range interface imperfections between the QW and surrounding barrier layers that have been found in the TEM micrographs. This gives the possibility to consider the whole QW layer as a sequence of individual quantum well cells of different width and hence, different effective mobility edge energies. Within each cell the short-range disorder, determined by short-range imperfections and/or alloy fluctuations, creates a variety of localized states. Such consideration gives the possibility to introduce two energy distributions with different energy scales: one for the effective mobility edges of the cells and another one for the localized states within each cell. Because of the finite lifetime and the finite lateral velocity, the whole hopping and recombination dynamics of the excitons are dominated by the particular cell, where the exciton was primarily created. Using the theoretical model with two scales of disorder, the main PL features of Ga(N,As,P)/GaP QW structures can be explained already even in case of completely "isolated" cells. A satisfactory simulation of all observed peculiarities in the PL behavior of Ga(N,As,P) quaternary alloys becomes possible by taking into account the exciton intercell transitions with temperature- and energy-dependent probabilities.

*christian.karcher@physik.uni-marburg.de

[1] J. Neugebauer and C. G. Van de Walle, Phys. Rev. B **51**, 10568 (1995).

[2] P. J. Klar, H. Grüning, M. Güngerich, W. Heimbrodt, J. Koch, T. Torunski, W. Stolz, A. Polimeni, and M. Capizzi, Phys. Rev. B **67**, 121206 (2003).

[3] W. Shan, W. Walukiewicz, J. W. Ager, E. E. Haller, J. F. Geisz, D. J. Friedman, J. M. Olson, and S. R. Kurtz, Phys. Rev. Lett. **82**, 1221 (1999).

[4] J. Wu, W. Shan, and W. Walukiewicz, Semicond. Sci. Technol. **17**, 860 (2002).

[5] M. R. Hofmann, N. Gerhardt, A. M. Wagner, C. Ellmers, F. Höhnsdorf, J. Koch, W. Stolz, S. W. Koch, W. W. Rühle, J. Hader, J. V. Moloney, E. P. O'Reilly, B. Borchert, A. Y. Egorov, H. Riechert, H. C. Schneider, and W. W. Chow, IEEE J. Quantum Electron. **38**, 213 (2002).

[6] P. J. Klar, H. Grüning, J. Koch, S. Schäfer, K. Volz, W. Stolz, W. Heimbrodt, A. M. Kamal Saadi, A. Lindsay, and E. P. O'Reilly, Phys. Rev. B **64**, 121203(R) (2001).

[7] W. Shan, W. Walukiewicz, K. M. Yu, J. Wu, J. W. A. III, E. E. Haller, H. P. Xin, and C. W. Tu, Appl. Phys. Lett. **76**, 3251 (2000).

[8] M. Güngerich, P. J. Klar, W. Heimbrodt, G. Weiser, J. F. Geisz, C. Harris, A. Lindsay, and E. P. O'Reilly, Phys. Rev. B **74**, 241202(R) (2006).

[9] B. Kunert, K. Volz, J. Koch, and W. Stolz, Appl. Phys. Lett. **88**, 182108 (2006).

[10] J. Chamings, A. R. Adams, S. J. Sweeney, B. Kunert, K. Volz, and W. Stolz, Appl. Phys. Lett. **93**, 101108 (2008).

[11] K. M. Yu, W. Walukiewicz, J. W. Ager III, D. Bour, R. Farshchi, O. D. Dubon, S. X. Li, I. D. Sharp, and E. E. Haller, Appl. Phys. Lett. **88**, 092110 (2006).

[12] J. Chamings, S. Ahmed, A. R. Adams, S. J. Sweeney, V. A. Odnoblyudov, C. W. Tu, B. Kunert, and W. Stolz, Phys. Status Solidi B, **246**, 527 (2009).

[13] S. D. Baranovskii, R. Eichmann, and P. Thomas, Phys. Rev. B **58**, 13081 (1998).

[14] O. Rubel, S. D. Baranovskii, K. Hantke, B. Kunert, W. W. Rühle, P. Thomas, K. Volz, and W. Stolz, Phys. Rev. B **73**, 233201 (2006).

[15] O. Rubel, M. Galluppi, S. D. Baranovskii, K. Volz, L. Geelhaar, H. Riechert, P. Thomas, and W. Stolz, J. Appl. Phys. **98**, 063518 (2005).

[16] H. Grüning, K. Kohary, S. D. Baranovskii, O. Rubel, P. J. Klar, A. Ramakrishnan, G. Ebbinghaus, P. Thomas, W. Heimbrodt, W. Stolz, and W. W. Rühle, Phys. Status Solidi C **1**, 109 (2004).

[17] O. Rubel, W. Stolz, and S. D. Baranovskii, Appl. Phys. Lett. **91**, 021903 (2007).

[18] B. Dal Don, K. Kohary, E. Tsitsishvili, H. Kalt, S. D. Baranovskii, and P. Thomas, Phys. Rev. B **69**, 045318 (2004).

[19] B. Kunert, K. Volz, J. Koch, and W. Stolz, J. Cryst. Growth **298**, 121 (2007).

[20] I. Németh, T. Torunski, B. Kunert, W. Stolz, and K. Volz, J. Appl. Phys. **101**, 123524 (2007).

[21] O. J. Glembocki and B. V. Shanabrook, Superlattices Microstruct. **5**, 603 (1989).

[22] S. D. Baranovskii and A. L. Efros, Sov. Phys. Semicond. **12**, 1328 (1978).

[23] A. Miller and E. Abrahams, Phys. Rev. **120**, 745 (1960).

[24] A. Žukauskas, K. Kazlauskas, G. Tamulaitis, M. A. Khan, J. W.

Yang, J. Zhang, G. Simin, M. S. Shur, and R. Gaska, Physica Status Solidi C **0**, 2737 (2003).

[25] K. Kazlauskas, G. Tamulaitis, A. Zukauskas, M. A. Khan, J. W. Yang, J. Zhang, G. Simin, M. S. Shur, and R. Gaska, Appl. Phys. Lett. **83**, 3722 (2003).

[26] K. Kazlauskas, G. Tamulaitis, P. Pobedinskas, A. Zukauskas, M. Springis, C.-F. Huang, Y.-C. Cheng, and C. C. Yang, Phys. Rev. B **71**, 085306 (2005).

[27] S. Imhof, A. Thränhardt, A. Chernikov, M. Koch, N. S. Köster, K. Kolata, S. Chatterjee, S. W. Koch, X. Lu, S. R. Johnson, D. A. Beaton, T. Tiedje, and O. Rubel, Appl. Phys. Lett. **96**, 131115 (2010).

[28] H. Tang, J. Phys.: Condens. Matter **15**, 8137 (2003).